Searching for ultralight dark matter with Mössbauer resonance*

Peng-Long Zhang (张朋龙)[1,2†] Yu-Ming Yang (杨玉明)[2,3] Xiao-Jun Bi (毕效军)[2,3] Qin Chang (常钦)[1,4]
Yu Gao (高宇)[2] Hai-Bo Li (李海波)[2,3] Wei Xu (徐伟)[2] Peng-Fei Yin (殷鹏飞)[2]

[1]Centre for Theoretical Physics, Henan Normal University, Xinxiang 453007, China
[2]Institute of High Energy Physics, Chinese Academy of Sciences, Beijing 100049, China
[3]School of Physical Sciences, University of Chinese Academy of Sciences, Beijing 100049, China
[4]Center for High Energy Physics, Henan Academy of Sciences, Zhengzhou 455004, China

Abstract: We investigate the feasibility of probing interactions between ultralight scalar dark matter and atomic nuclei using stationary Mössbauer spectroscopy. The exceptional energy resolution of the Mössbauer resonance enables searches for minute nuclear energy shifts induced by the local dark matter field. The dark matter mass range considered in this work is 10^{-18}–10^{-8} eV. We present projected constraints for two candidate Mössbauer isotopes, ^{109}Ag and ^{45}Sc, with ^{109}Ag providing the strongest sensitivity. For ^{109}Ag, projected sensitivities of approximately 10^{-19}, 10^{-22}, and 10^{-21} GeV^{-1} can be achieved for the scalar DM–photon, DM–gluon, and DM–quark couplings f_γ^{-1}, f_g^{-1}, and $f_{\hat{m}}^{-1}$, respectively. In the low-mass region, the projected sensitivity to the scalar DM–photon coupling approaches current constraints from equivalence-principle (EP) tests. These results demonstrate that Mössbauer-based techniques provide a promising and competitive approach to probing ultralight dark matter interactions with Standard Model particles.

Keywords: scalar dark matter, Mössbauer resonance, a stationary Mössbauer spectroscopy scheme, nuclear energy shifts

DOI: 10.1088/1674-1137/ae9279 **CSTR:** 32044.14.ChinesePhysicsC.50113101

I. INTRODUCTION

Understanding the fundamental nature of dark matter remains one of the most profound open questions in modern physics. Although dark matter constitutes approximately 26.8% of the total energy density of the Universe–making it roughly five times more abundant than ordinary (baryonic) matter [1]–its microscopic properties and interactions remain undetected. Evidence for dark matter primarily arises from its gravitational effects on galactic and cosmological scales [1−6], yet all attempts to directly observe its non-gravitational interactions with Standard Model particles have so far yielded null results.

Among the broad range of dark matter candidates, ultralight dark matter (ULDM) has attracted increasing attention. This class of models postulates bosonic fields with masses spanning a wide range, from $m \sim 10^{-23}$eV up to 1 eV [7]. In many realizations–such as axions, axion-like particles, and scalar dark matter–the ULDM field behaves as a coherently oscillating classical wave, giving rise to distinctive experimental signatures. These particles often couple feebly to photons, electrons, or nucleons, potentially inducing time-varying fundamental constants or energy-level shifts in atomic and nuclear systems [8−17].

The Mössbauer effect [18] is well known for its exceptional energy resolution in recoil-free nuclear gamma-ray resonance. A classic application is the experimental verification of the gravitational redshift of photons in the Earth's gravitational field [19, 20]. Over the years, the Mössbauer effect has had a profound impact on materials science and chemistry. Its extremely high energy resolution also makes it a promising tool for probing tiny shifts in nuclear transition energies induced by couplings to a time-varying dark matter (DM) field. Such couplings can lead to small but measurable modifications of nuclear binding energies, resulting in shifts of the resonance lines in the Mössbauer spectrum. Importantly, the magnitude of these shifts is determined by the strength of the new in-

Received 4 January 2026; Accepted 29 July 2026; Accepted manuscript online 30 July 2026

* Supported by the National Natural Science Foundation of China (12175248, 12447105, 12275067), the Science and Technology R&D Program Joint Fund Project of Henan Province (225200810030), the Science and Technology Innovation Leading Talent Support Program of Henan Province, and the National Key R&D Program of China (2023YFA1606000, 2023YFA1608903)

† E-mail: 2102084002@stu.htu.edu.cn

Content from this work may be used under the terms of the Creative Commons Attribution 3.0 licence. Any further distribution of this work must maintain attribution to the author(s) and the title of the work, journal citation and DOI. Article funded by SCOAP[3] and published under licence by Chinese Physical Society and the Institute of High Energy Physics of the Chinese Academy of Sciences and the Institute of Modern Physics of the Chinese Academy of Sciences and IOP Publishing Ltd

teraction, while electromagnetic effects on nuclear energy levels are significantly suppressed by shielding from the electron cloud. In addition, electromagnetic contributions typically couple to nuclear moments, which are themselves suppressed by the small size of the nucleus.

Recently, Refs. [21−23] explored the use of the Mössbauer effect as a tool to search for new physics. In Ref. [21], the authors proposed exploiting the ultrahigh energy resolution of Mössbauer spectroscopy to probe short-range interactions through tiny shifts in nuclear energy levels. They considered two complementary implementations: traditional radioactive Mössbauer sources and synchrotron-radiation-based excitation schemes. This approach significantly enhances sensitivity to new interactions at nanometer to micrometer scales and provides a unique probe of the underlying microscopic couplings and nuclear structure effects. Ref. [23] focuses on using synchrotron-radiation Mössbauer spectroscopy to detect ultralight scalar dark matter through modulations in the absorption spectrum over large source–absorber baselines. Ref. [22] proposes a stationary Mössbauer scheme based on the ^{109}Ag isotope. In this setup, perturbations from high-frequency gravitational waves under the local gravitational field can induce vertical shifts in the Mössbauer resonance height. The authors demonstrate that the ultrahigh energy resolution of Mössbauer spectroscopy enables competitive sensitivity to gravitational waves across a wide frequency range, from kHz to above MHz. In this work, we explore the sensitivity of ultralight scalar dark matter searches using a recently proposed static scheme [22]. Our analysis considers two radioactive Mössbauer isotopes, ^{109}Ag and ^{45}Sc, as well as an X-ray free-electron-laser (XFEL)-based Mössbauer source using ^{45}Sc.

The rest of this paper is organized as follows. In Sec. II, we describe the dark-matter-induced shift in nuclear energy levels and discuss the choice of Mössbauer nuclei used in our analysis. In Sec. III, we introduce the stationary Mössbauer spectroscopy scheme for dark matter searches. In Sec. IV, we use Monte Carlo simulations and a χ^2 analysis to estimate the dark-matter-induced shift in the absorber's resonance position, represented by a vertical displacement ΔZ_0. In Sec. V, we present the interaction Lagrangian for dark matter couplings to photons, gluons, and quarks, and calculate the resulting small shifts in nuclear energy levels. In Sec. VI, we combine theoretical estimates with Monte Carlo simulations to derive projected constraints on the coupling parameters between dark matter and photons, gluons, and quarks. Finally, in Sec. VII, we present our conclusions.

II. DARK MATTER INDUCED ENERGY SHIFTS AND NUCLEAR SELECTION

In the ultralight bosonic dark matter scenario, galactic dark matter behaves as a coherently oscillating classical scalar field with a central frequency determined by the nonrelativistic particle energy, $\omega_\phi = m_\phi + O(\beta^2)$, and a correspondingly small energy dispersion, $\sigma(\omega) \sim \beta^2 m_\phi$. Within one coherence timescale, the local dark matter field value can be written as

$$\phi(t,\vec{x}) \simeq \frac{\sqrt{2\rho_{\rm DM}}}{m_\phi}\cos\left(\omega_\phi t - m_\phi\vec{\beta}\cdot\vec{x}\right), \tag{1}$$

where $\rho_{\rm DM} \sim 0.4\,{\rm GeV/(cm)^3}$ is the local dark matter density, $|\beta| \sim 10^{-3}$ is the virial velocity, and $\omega_\phi \approx m_\phi$. The dark-matter-induced shift in the nuclear transition energy is proportional to the dark matter field. Thus, the energy-level shift of the emitter at position $\vec{x} = \vec{0}$ and time t is $\kappa\phi(t,\vec{0})$. When the photon reaches the absorber located at $\vec{x} = \vec{L}$, the corresponding shift is $\kappa\phi(t+L,\vec{L})$. The resulting difference between the emitter and absorber transition energies is given by

$$\begin{aligned}\Delta E &= \kappa\phi(t+L,\vec{L}) - \kappa\phi(t,\vec{0})\\ &= \kappa\frac{\sqrt{2\rho_{\rm DM}}}{m_\phi}\cos\left(\omega_\phi(t+L)) - m_\phi\vec{\beta}\cdot\vec{L}\right)\\ &\quad - \kappa\frac{\sqrt{2\rho_{\rm DM}}}{m_\phi}\cos\left(\omega_\phi t - m_\phi\vec{\beta}\cdot\vec{0}\right)\\ &= -2\kappa\frac{\sqrt{2\rho_{\rm DM}}}{m_\phi}\sin\left(\frac{m_\phi L(1-\beta)}{2}\right)\\ &\quad\times\sin\left(m_\phi\left[t+\frac{L(1-\beta)}{2}\right]\right).\end{aligned} \tag{2}$$

In a Mössbauer measurement, the small energy shift predicted here can be resolved with exceptional precision.

While ^{57}Fe is currently the most widely used nucleus in Mössbauer spectroscopy, several other isotopes are known to exhibit even narrower resonance lines [24]. Among them, the 93-keV transition in ^{67}Zn, with a fractional linewidth of $\Gamma_0/E_0 \sim 10^{-15}$ [25], has been successfully used in high-resolution Mössbauer spectroscopy, particularly in gravitational redshift experiments [19, 20]. This demonstrates the potential of narrow-linewidth nuclear transitions for precision measurements.

Motivated by this potential, isotopes with even narrower intrinsic linewidths have attracted increasing attention. For instance, the $E_0 = 88$ keV transition in ^{109}Ag has an extremely small natural width Γ_0 and can, in principle, achieve an extraordinarily small fractional linewidth of $\Gamma_0/E_0 \sim 10^{-22}$. This enables unprecedented spectroscopic resolution and has been proposed for detecting gravitational effects at small scales [22].

Another particularly promising candidate is ^{45}Sc, which exhibits a nuclear transition at 12.4 keV with an isomeric lifetime of $\tau_0 = 0.47$ s and a natural linewidth of

$\Gamma_0 = \hbar/\tau_0 = 1.4$ feV, corresponding to an extraordinarily high quality factor of $Q = E_0/\Gamma_0 \simeq 10^{19}$. However, unlike some other Mössbauer isotopes, the application of ^{45}Sc is limited by the relatively small branching ratio for the β^- decay of its parent nucleus, ^{45}Ca, into the excited state relevant to the Mössbauer transition. This small branching ratio suppresses the achievable resonant photon flux from radioactive sources.

Earlier attempts to achieve resonant excitation of ^{45}Sc at third-generation synchrotron radiation facilities were unsuccessful because of insufficient spectral flux. This limitation has only recently been overcome with the advent of narrow-band, high-repetition-rate X-ray free-electron lasers (XFELs), most notably the European XFEL [26–28], where resonant excitation of ^{45}Sc has been demonstrated. Next-generation facilities, such as the Shanghai High Repetition Rate XFEL and Extreme Light Facility (SHINE) [29–31] and the Shenzhen Superconducting Soft X-ray Free Electron Laser (S^{3}FEL) [32, 33], are currently under construction and are expected to provide high-brightness, high-repetition-rate X-ray beams suitable for resonant nuclear excitation.

In this work, we focus on ^{109}Ag and ^{45}Sc as benchmark isotopes to investigate the projected sensitivity of Mössbauer measurements to shifts in nuclear transition energies induced by ultralight dark matter through recoil-free photons. Key nuclear parameters of these isotopes are summarized in Table 1, including the transition energy (E_0), natural linewidth (Γ_0), fractional linewidth (Γ_0/E_0), natural lifetime, experimentally achieved resonance width ($\Gamma_{\rm exp}$), and radioactive parent-nucleus lifetime.

Table 1. Properties of selected Mössbauer isotopes, ^{109}Ag and ^{45}Sc, including nuclear transition energy E_0, natural linewidth Γ_0, the ratio Γ_0/E_0, natural lifetime, experimentally achieved resonance width $\Gamma_{\rm exp}$, and the lifetime of the radioactive parent nucleus. The experimentally achieved resonance width for ^{45}Sc is adopted from observations. For ^{109}Ag, we assume 1.9×10^{-16} eV for the estimate [22]. * Spontaneous ^{45}Ca $\rightarrow^{45}$ Sc decay has a large branching-fraction suppression, $O(10^{-5})$, to the first ^{45}Sc excited state. Here, we list ^{45}Sc as a candidate because of recent success at XFEL.

Isotope	Nuclear transition energy E_0/keV	Natural Width Γ_0/eV	Γ_0/E_0	Lifetime	$\Gamma_{\rm exp}$/eV	Parent lifetime/d
^{109}Ag	88	2.3×10^{-17}	1.2×10^{-22}	27.6 s	1.9×10^{-16}	461 (^{109}Cd)
^{45}Sc	12.4	1.4×10^{-15}	1.1×10^{-19}	0.47 s	7.0×10^{-13} [34]	163 (^{45}Ca)*

III. THE STATIONARY SCHEME

To probe possible variations in nuclear transition energies induced by an oscillating dark matter background, we consider a static measurement scheme based on a Mössbauer resonance absorber with an ultranarrow linewidth [22]. As illustrated in Fig. 1, a fixed baseline L is established between the emitter and the absorber, with the absorber and detector arranged along the vertical direction. The right panel schematically shows the absorption spectrum measured by the detector. In the presence of the Earth's gravitational field, the displacement of the absorption peak can be used to infer the nuclear energy shift.

Under standard Mössbauer resonance conditions, when the emitter and absorber are located at the same gravitational potential, i.e., at the same height Z_0, the nuclear transition energies of the source and absorber are precisely matched. This allows the emitted photons to be resonantly absorbed without recoil. If dark matter couples to nucleons, it can induce minute shifts in the nuclear energy levels, producing a small energy offset ΔE in the emitted photons. In this case, an absorber placed at the same height no longer satisfies the resonance condition, and resonant absorption is suppressed. Consequently, more photons pass through the absorber and are recorded by the detector.

Resonance can be restored by exploiting the gravitational redshift effect to compensate for the energy mismatch. In the Earth's gravitational field, the photon energy changes as the photon propagates in the vertical direction. Thus, introducing a small vertical displacement ΔZ of the absorber creates a difference in gravitational potential, which induces a corresponding redshift or blue-

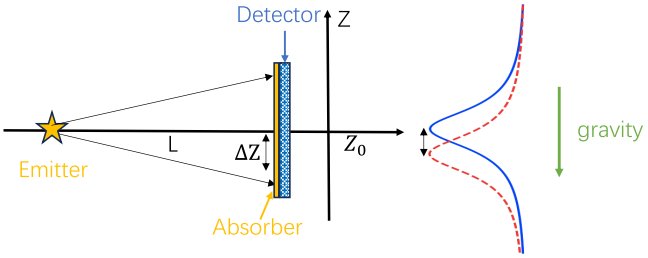


Fig. 1. (color online) Schematic of the static Mössbauer measurement for detecting dark-matter-induced energy shifts. The emitter and absorber are separated by a fixed baseline L, while the absorber is vertically displaced by ΔZ to compensate for the energy mismatch through gravitational redshift. The absorption spectrum measured by the detector is shown schematically; the shift of the resonance peak is used to infer the corresponding energy offset ΔE.

shift in the photon energy. In the weak-field limit near the Earth's surface, the relation between the energy shift and the vertical displacement is given by

$$\frac{\Delta E}{E} \simeq \frac{g\Delta Z}{c^2}, \tag{3}$$

where g is the gravitational acceleration and E is the photon energy. When the gravitationally induced shift compensates for the dark-matter-induced energy offset ΔE, resonance is restored at the displaced position. Thus, by measuring the vertical displacement ΔZ at which resonant absorption is maximized, for example, by scanning the absorption line, one can infer the corresponding energy shift ΔE, thereby providing a means to probe or constrain the coupling between dark matter and nuclear energy levels.

Let us assume that the emitter is stationary at a vertical position Z_S. The emission line of the source is narrow and unsplit, with a natural linewidth Γ. The measured spectral lineshape is Lorentzian and centered at the resonance energy E_0. Denoting the total photon emission rate of the source as N_0, the differential number of recoil-free photons with energy E_γ emitted per unit energy and time is given by [22, 35]:

$$N_{\rm RF}(E) = N_0 f_S \cdot \frac{\Gamma/2\pi}{[E-E_0]^2+(\Gamma/2)^2}, \tag{4}$$

where f_S is the recoil-free fraction of the source emission.

To achieve the desired performance in a static configuration, the detector must have high spatial resolution, and the finite sizes of the absorber and detector should enable them to cover a narrow vertical range. In this configuration, the Mössbauer transmission function can be formulated by replacing the conventional Doppler shift with a gravitationally induced energy correction arising from the vertical displacement. The transmission function $C(Z)$ at a detector height Z is:

$$\begin{aligned} C(Z) =& N_0\, \mathrm{e}^{-\mu_e t'} \cdot \Big[(1-f_S) + \int_{-\infty}^{\infty} f_S \xi(Z_S, E_0) \\ & \cdot \mathrm{e}^{-t\xi(Z, E_0+\Delta E_0)\Gamma/2\pi} \mathrm{d}E\Big], \end{aligned}$$

$$\xi(Z, E_0) \equiv \frac{\Gamma/2\pi}{[E-g(Z-Z_S)E-E_0]^2+(\Gamma/2)^2}. \tag{5}$$

Here, ΔE_0 represents the intrinsic energy offset between the emitter and absorber, which can be compensated by a small vertical height difference within the detector range. At resonance, this correction satisfies $g\langle Z-Z_S\rangle E = -\Delta E_0$, and we define the corresponding central detection height as $Z_0 = \langle Z\rangle$ for convenience. The attenuation factor $e^{-\mu_e t'}$ accounts for non-resonant absorption, where t' is the absorber thickness expressed as the area density, *i.e.*, $t' = \rho L$, with units of $\mathrm{g\,cm^{-2}}$ [35], and μ_e is the mass absorption coefficient at resonance. The effective resonant optical depth is $t = f_A N_M \sigma_0$, where f_A is the recoil-free fraction of the absorber, N_M is the number of Mössbauer nuclei per unit area, which increases with absorber thickness, and σ_0 is the peak resonant cross section.

For practical calculations, the transmission function can be approximated using a simplified parameterization that emphasizes the gravitational energy shift [22]:

$$C(Z) = N_0\, \mathrm{e}^{-\mu_e t'} \left\{1 - f_S\, \epsilon \cdot \frac{\Gamma_{\rm exp}^2}{[g(Z-Z_0)E_0]^2+\Gamma_{\rm exp}^2}\right\}. \tag{6}$$

Here, ϵ is the effective resonant absorption fraction, and $\Gamma_{\rm exp}$ is the observed linewidth after transmission through the absorber. Both quantities depend nontrivially on the absorber thickness. The quantity f_S represents the fraction of recoil-free emission, whereas $f_S\epsilon$ represents the total recoil-free absorption fraction.

We consider a factor that induces a frequency shift $\Delta f(t)$ in the resonant absorption of photons by the absorber. This shift results in a vertical displacement of the resonance position, given by

$$Z_0 \to Z_0(t) = Z_0 + g^{-1}\frac{\Delta f(t)}{f_\gamma}. \tag{7}$$

We define the displacement as $\Delta Z_0(t) \equiv Z_0(t) - Z_0$. This spatial shift can be inferred from variations in the Mössbauer absorption efficiency at the detector. If the spatial resolution is sufficiently high, both $\Delta Z_0(t)$ and the corresponding $\Delta f(t)$ can be measured with a sensitivity exceeding the effective Mössbauer linewidth, $\Gamma_{\rm exp}/E_0$.

IV. DARK MATTER SIGNAL

The interaction between oscillating dark matter and atomic nuclei can induce small shifts in nuclear energy levels. This, in turn, produces a slight change in the resonance absorption energy observed in the Mössbauer effect, leading to a vertical displacement of the absorber's resonance absorption position, denoted as $Z_0(t) - Z_0$. This vertical displacement, ΔZ_0, is quantitatively related to the shift in resonance energy, ΔE, by the following relation:

$$\Delta Z_0 \equiv Z_0(t) - Z_0 = g^{-1}\frac{\Delta f(t)}{f_\gamma} = g^{-1}\frac{\Delta E}{E_0}. \tag{8}$$

The 88 keV emission line of ^{109}Ag has a natural linewidth of 2.3×10^{-17} eV [21, 24]. When both emission and absorption processes are considered, the ideal resonance width effectively doubles. This ^{109}Ag linewidth cor-

responds to a vertical displacement of approximately 20 μm in Earth's gravitational field, with $g = 9.8\ \mathrm{m/s^2}$. To ensure precise localization, the detector is designed with a spatial resolution of 10 μm, which is half the broadened absorption peak width. We further assume that the detector maintains high efficiency, approaching 100%, for detecting these high-energy X-ray photons.

The resonance strength is inferred by measuring the transmitted, unabsorbed photon flux through an absorber layer as a function of the vertical position Z. The absorption fraction is given by Eq. (6), which predicts a position-dependent suppression of the photon flux near the resonance. To quantify this effect, we discretize the detector along the vertical direction into bins of width δZ. The detector therefore measures a binned spatial distribution of photon counts. We denote by $C_i(Z_i;Z_0)$ the expected number of photon counts in the ith bin centered at position Z_i, where Z_0 specifies the location of the resonance peak. Here, Z_i denotes the fixed central position of the ith bin and is not a free parameter in the fit. Far from the resonance region, absorption becomes negligible, and the count rate approaches an asymptotic value C_∞, corresponding to the unperturbed photon flux.

For a given Mössbauer source, the bin width is chosen to match the characteristic spatial scale over which the resonance varies because of gravitational energy shifts. Specifically, we set $\delta Z \sim \Gamma_{\mathrm{exp}}/gE_0$, and adopt $\delta Z/2 = 10$ μm for ^{109}Ag, ensuring that the resonance profile is adequately resolved without introducing unnecessary statistical fluctuations.

In the Monte Carlo simulation, the simulated data C_i^{exp} are generated by drawing from a Poisson distribution with a mean given by the theoretical expectation $C_i(Z_i;Z_0^{\mathrm{true}})$. We set $Z_0^{\mathrm{true}} = 0$, which defines the origin of the spatial coordinate. Because the model depends only on the relative displacement $Z - Z_0$, this choice does not affect the statistical uncertainty and allows the fitted value to be interpreted directly as the deviation from the true resonance position.

Because the expected counts $C_i(Z_i;Z_0)$ depend on the resonance position Z_0, we determine the best-fit value of Z_0 by minimizing the following χ^2 function:

$$\chi^2(Z_0) = \sum_i \frac{\left[C_i(Z_i;Z_0) - C_i^{\mathrm{exp}}\right]^2}{\Delta_i^2}, \tag{9}$$

where C_i^{exp} denotes the observed number of counts in the ith bin. In this analysis, Z_0 is treated as the only free parameter, whereas all other quantities are fixed. We emphasize that the above χ^2 definition does not include detector effects or systematic uncertainties (e.g., through nuisance or pull terms) and therefore corresponds to an idealized, statistics-dominated scenario.

The above χ^2 definition corresponds to a maximum-likelihood estimator under the assumption that the statistical fluctuations in each bin are approximately Gaussian. This approximation is justified because the photon counts in each bin follow a Poisson distribution, which approaches a Gaussian distribution with variance equal to its mean for sufficiently large counts. Accordingly, in the statistics-dominated regime, we take $\Delta_i = \sqrt{C_i}$, where C_i represents the expected counts in the ith bin.

The spatial resolution of the resonance position Z_0 is then determined from the curvature of the likelihood function, or equivalently the χ^2 function, around its minimum. In practice, this corresponds to the statistical uncertainty of the fitted parameter Z_0, which can be extracted either from the second derivative of χ^2 or from repeated Monte Carlo realizations of the experiment.

The simulated position resolution of the Lorentzian peak is shown in Fig. 2. For ^{109}Ag, the experimental linewidth is 20 μm, and the bin width along the z-axis is 10 μm. In each bin, the number of incident 88 keV photons is determined by the intensity and distance of the source. The recoil-free fraction is set to $f_S = 0.5$, and the absorption fraction is taken to be $\epsilon = 0.8$, corresponding to a near-optimal absorber configuration [22]. The photon flux measured in the resonance bins decreases because of resonance absorption, as shown by the simulated photon counts in Fig. 2. We note that $f_S = 0.5$ is an unphysical value adopted solely for illustrative purposes to enhance the visibility of the absorption profile in this simulation. For the final sensitivity estimates presented in this work, we use the experimentally measured value $f_S = 0.05$ for ^{109}Ag.

For our analysis, we assume that the absorbers and detectors are uniformly arranged on a circle, with the ra-

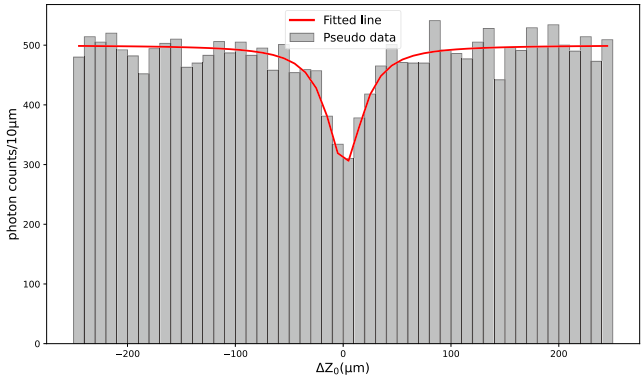


Fig. 2. (color online) For the ^{109}Ag nucleus: simulated peak-position accuracy ΔZ_0 obtained from a single pseudo-experiment measuring the position of the absorption Lorentzian peak, assuming an experimental linewidth of 20 μm, a z-axis bin width of 10 μm, 500 arriving photons per bin, a recoil-free fraction f_S =0.5, and an absorption fraction ϵ=0.8. The value f_S=0.5 is unphysical and is adopted solely to improve the visibility of the absorption profile in this illustrative simulation.

dioactive emitter positioned at the geometric center. The angular coverage θ corresponding to the vertical height difference ΔZ_0 of the resonant absorption peaks on the detector is given by

$$\theta = \arctan\left(\frac{\Delta Z_0}{L}\right), \tag{10}$$

where L denotes the distance between the source and the absorber. In our setup, we set $L = 1\,m$. For a circular detector geometry, the fraction of the total solid angle subtended by the detector is given by

$$f_\theta = \frac{2\pi\theta}{4\pi} = \frac{\theta}{2}. \tag{11}$$

This quantity represents the effective detection solid-angle coverage normalized to the full solid angle of 4π steradians.

We consider a radioactive source with an activity of $A = 0.1$ Ci (corresponding to 3.7 GBq). The total number of photons emitted during the measurement is

$$N_{\rm total} = A \times P_\gamma \times f_{\rm BR} \times \Delta t \times N_{\rm exp}, \tag{12}$$

where $P_\gamma = 1/(1+\alpha_{\rm T})$ is the photon emission probability, and $\alpha_{\rm T}$ is the internal conversion coefficient, defined as the ratio of the number of internal conversion electrons $N_{\rm IC}$ to the number of gamma emissions N_γ. The quantity $f_{\rm BR}$ denotes the branching ratio for the transition of interest, and $\Delta t = T/3$ is the integration time per data segment, with $T = 2\pi/m_\phi$ being the oscillation period associated with dark matter of mass m_ϕ. The choice $\Delta t = T/3$ represents a compromise between time resolution and photon statistics. A substantially longer integration time would average out the oscillatory signal, whereas a much shorter one would reduce the photon counts per bin and thereby degrade the statistical sensitivity. This choice ensures that the modulation induced by dark matter oscillations remains resolvable and is not washed out. The factor $N_{\rm exp} = 10^6$ accounts for the statistical enhancement arising from the number of dark matter oscillation periods within its coherence time scale. Here, the coherence time is taken to correspond to a single data-taking period. We take the DM coherence time scale $t_c = N_{\rm exp} \cdot 2\pi m_\phi^{-1}$ as the benchmark coherent measurement time in this sensitivity estimate; longer data-taking periods are treated as repeated but independent measurements. For each energy bin, the number of photons contributing to that bin is

$$N_\gamma = N_{\rm total} \times f_\theta. \tag{13}$$

This framework provides a quantitative estimate of the photon statistics available per bin under realistic experimental conditions, which is crucial for determining the achievable measurement sensitivity.

For ^{45}Sc, two approaches can be used to generate Mössbauer radiation. The conventional approach assumes a radioactive ^{45}Ca source with an activity of 0.1 Ci. However, the direct use of ^{45}Ca is inefficient because it almost always decays to the ground state of ^{45}Sc. An alternative approach uses synchrotron radiation to resonantly excite the ^{45}Sc nucleus, for example, with a high-intensity X-ray beam [26]. Resonant excitation of ^{45}Sc by an XFEL beam generates coherently scattered photons in the forward direction [36]. The yield of pure nuclear-resonant photons can be estimated from the incident photon flux within the narrow resonance bandwidth. Owing to the relatively long lifetime of ^{45}Sc (0.47 s), the nuclear-resonant signal can be effectively distinguished from the directly transmitted incident beam. The beam-excited Mössbauer resonance photon flux $N_\gamma^{\rm MS}$ can be estimated as

$$N_\gamma^{\rm MS} = N_\gamma^{\rm SR}\frac{\Gamma}{\Delta E^{\rm SR}}, \tag{14}$$

where $N_\gamma^{\rm SR}$ denotes the spectral photon flux of the synchrotron radiation, Γ is the natural linewidth of the ^{45}Sc nuclear transition, and $\Delta E^{\rm SR}$ represents the energy resolution of the synchrotron source.

The resonant photons are emitted within a narrow angular distribution and, in principle, can be collected efficiently by the absorber or detector. In addition, coherent forward scattering induced by synchrotron excitation strongly collimates the emitted photons in the forward direction. In our setup, the detectors are placed along the forward direction, and optical elements can be used to adjust the beam spot size to match the detector acceptance. Therefore, for the purpose of sensitivity estimation, we assume an idealized configuration in which most Mössbauer photons produced via synchrotron radiation are received by the absorber or detector.

To estimate the photon statistics at the absorber, we approximate the transverse beam profile as uniform over an effective illuminated area. The number of photons intercepted by the absorber is then given by the ratio of the detector area to the beam spot area. Specifically, the absorber acceptance can be written as

$$f_{\rm geo} = \frac{A_{\rm abs}}{A_{\rm beam}} = \frac{hx}{\pi r^2}, \tag{15}$$

where h and x denote the vertical and horizontal dimensions of the absorber or detector, respectively, and R is the effective beam spot radius at the detector location. In our setup, we consider a vertical separation of $h \approx \Delta Z =$

0.26 m and a detector width of $x = 0.1$ m. To ensure full coverage of the vertically distributed absorbers/detectors, we conservatively assume a beam spot radius of $R \approx \Delta Z$. Under this assumption, the geometrical acceptance reduces to

$$f_{\rm geo} \approx \frac{x}{\pi \Delta Z}. \tag{16}$$

Accordingly, the number of photons incident on the absorber can be estimated as

$$N_\gamma = N_\gamma^{\rm MS} \times f_{\rm geo} \times P_\gamma \times \Delta t \times N_{\rm exp}. \tag{17}$$

We note that this estimate corresponds to an idealized configuration with a uniform beam profile. In practice, the beam profile can be tailored using X-ray optics to control its spatial distribution and divergence. For example, defocused illumination or beam-shaping techniques can be used to adjust the beam size and improve overlap with the detector geometry, thereby enhancing the effective photon collection efficiency [37–38]. In our analysis, we adopt an effective beam energy resolution of $\Delta E^{\rm SR} = 1$ eV for a modern synchrotron radiation source, such as the European XFEL [26–28], and a spectral photon flux of $N_\gamma^{\rm SR} = 5 \times 10^{14}\,{\rm ph\,s^{-1}\,eV^{-1}}$ [26].

To ensure that the signal-to-noise ratio reaches at least 3σ, the number of detected signal and background events must satisfy:

$$\frac{N_S}{\sqrt{N_S + N_B}} \geq 3\sigma, \tag{18}$$

where N_S denotes the number of signal events and is given by $N_S = \epsilon f_S N_\gamma$. The remaining events are treated as background; thus, the background count is $N_B = N_\gamma - N_S$. Substituting these expressions into Eq. (18) and solving for the total number of detected photons, N_γ, yields the minimum number of photons required to achieve a 3σ detection significance:

$$N_\gamma \geq \left(\frac{3\sigma}{\epsilon f_S}\right)^2. \tag{19}$$

This condition sets a lower bound on the total number of photons that must be collected for the signal to be statistically distinguishable from the background at the desired confidence level.

Generally, one must balance a larger absorption fraction against mass attenuation. Ref. [39] showed that a mass attenuation of approximately $\mu_e t' \approx 2$ provides optimal sensitivity, corresponding to an absorber efficiency of $\epsilon \approx 0.8$ [22]. For ^{109}Ag, we adopt a recoil-free fraction of $f_S = 0.05$ [40] and an absorption fraction of $\epsilon = 0.8$. We determine the fitted ΔZ_0 using the χ^2 function defined in Eq. (9). For each simulated dataset, χ^2 is constructed by comparing the expected counting rate as a function of Z with the mock data, accounting for the statistical uncertainty in each bin. The best-fit value of ΔZ_0 is then obtained by minimizing the χ^2 function with respect to this single parameter. An example fit from one representative simulation is shown in Fig. 2. To estimate the statistical uncertainty, we perform 1000 independent Monte Carlo realizations and extract the 95% confidence interval for ΔZ_0 from the distribution of best-fit values across all simulations.

The resulting 95% confidence interval on ΔZ_0 is then translated into the corresponding shift in the resonance absorption energy using Eq. (8), which encodes the dark matter-induced modulation of the resonance condition. Combining this result with the theoretical relations in Eqs. (21), (22), and (23), we derive constraints on the couplings between dark matter and Standard Model particles, including photons, quarks, and gluons. This procedure establishes a direct link between the experimentally accessible observable and the underlying dark matter parameters, allowing the projected sensitivity to be interpreted as bounds on dark matter interactions.

We extend the methodology previously applied to the ^{109}Ag nucleus to an additional emitter, ^{45}Sc. For ^{45}Sc, the 12.4 keV nuclear transition has an experimentally achieved linewidth of 7.0×10^{-13} eV [34], corresponding to a vertical energy shift of approximately $\delta Z = 0.52$ m in Earth's gravitational field. To resolve this gravitationally induced broadening, the detector is designed with a spatial resolution of 0.26 m, *i.e.*, half of the broadened absorption width. The Lamb–Mössbauer factor at room temperature, estimated within the Debye approximation, is approximately 0.75 [26] for ^{45}Sc. In this case, we employ a χ^2-minimization procedure to extract the best-fit vertical displacement Z_0. Based on 1000 Monte Carlo simulations, we determine the 95% confidence interval for ΔZ_0.

Table 2 summarizes the key nuclear parameters of these isotopes, including the internal conversion coefficient $\alpha_{\rm T}$ [41], gamma-emission probability P_γ, branching ratio $f_{\rm BR}$ [41], recoil-free fraction f_S, and absorption fraction ϵ, which is taken to be 0.8.

V. DARK MATTER - NUCLEUS INTERACTIONS

In this section, we examine how dark matter interactions with photons, quarks, and gluons can affect the energy levels of atomic nuclei. We present the corresponding Lagrangians for each interaction type and derive formulas for the resulting nuclear energy shifts.

To describe the interaction between the ultralight dark matter field ϕ and the Standard Model, we consider a lin-

Table 2. Properties of the selected Mössbauer isotopes ^{109}Ag and ^{45}Sc, including the internal conversion coefficient α_T, gamma-ray emission probability P_γ, branching ratio f_{BR}, recoil-free fraction f_S, and absorption fraction $\epsilon = 0.8$ throughout.

Isotope	α_T	P_γ	f_{BR}	f_S
^{109}Ag	26.3	0.037	1	0.05
^{45}Sc	423	0.0024	2×10^{-5}	0.75

ear coupling of ϕ to quarks (q), gluons ($G_{a\mu\nu}$), and photons ($F_{\mu\nu}$). The corresponding interaction Lagrangian is given by [21, 23]:

$$\mathcal{L} \supset \sum_{\psi=u,d} -\frac{\phi}{f_\psi} m_\psi \bar{\psi}\psi - \frac{\phi}{4f_\gamma}F^2 - \frac{\phi}{4f_g}G^2, \tag{20}$$

where $G^2 = G^a_{\mu\nu}G^{a\mu\nu}$, with a the color index; $F^2 = F_{\mu\nu}F^{\mu\nu}$; and f_ψ, f_γ, and f_g denote the interaction strengths with the various sectors.

These interactions can induce time-dependent variations in fundamental constants and parameters, such as the fine-structure constant α, the down-quark mass, and the strong coupling constant α_s. Such variations shift nuclear energy levels, which can be estimated for each type of coupling.

Photon coupling: The coupling $\frac{\phi}{4f_\gamma}F^2_{\mu\nu}$ shifts the fine-structure constant as $\alpha \to \alpha - \frac{\alpha^2\phi}{4f_\gamma}$, thereby altering the electromagnetic self-energy of the nucleus. For a nucleus with Z protons and mass number A, the resulting energy shift is approximately [21, 23]

$$\Delta E \simeq -\frac{Z\alpha^2}{A^{1/3}r_0}\frac{\Delta\phi}{f_\gamma}, \tag{21}$$

where $r_0 \approx 1.2\,\mathrm{fm}$ is a typical nuclear length scale.

Quark (Yukawa) coupling: We consider a linear Yukawa coupling between the scalar field ϕ and light quarks in the isospin-symmetric basis, where $\hat{m} = (m_u + m_d)/2$. This interaction induces a fractional variation $\Delta\hat{m}/\hat{m} = \phi/f_{\hat{m}}$, which propagates to the pion mass through $m_\pi^2 \propto \hat{m}$ and thereby modifies pion-mediated nuclear forces. To estimate the resulting shift in nuclear energy, we employ the one-pion-exchange (OPE) potential between nucleons. For internucleon distances $r \lesssim 1/m_\pi$, the induced energy shift can be approximated as [23]

$$\Delta E \simeq 12.3\,\mathrm{MeV}\,\frac{\Delta\phi}{f_{\hat{m}}}. \tag{22}$$

Gluon coupling: The coupling $\frac{\phi}{4f_g}G^2_{\mu\nu}$ shifts the QCD coupling constant as $\alpha_s \to \alpha_g - \frac{\alpha_s\phi}{4f_g}$. The induced energy shift is approximately [21]

$$\Delta E \simeq 0.08\,\mathrm{GeV}\,\frac{\Delta\phi}{f_g}. \tag{23}$$

VI. PROJECTED SENSITIVITY

We investigate the parameter space for each interaction channel by equating the dark matter–induced energy shifts, given in Eqs. (21), (22), and (23), to the experimentally accessible shift described in Eq. (8). An emitter source with an activity of $A = 0.1$ Ci (3.7 GBq) is located at the center, while the absorber and detectors are uniformly distributed along a circle of radius $L = 1\,m$ for ^{109}Ag and ^{45}Sc. Under these conditions, we derive the

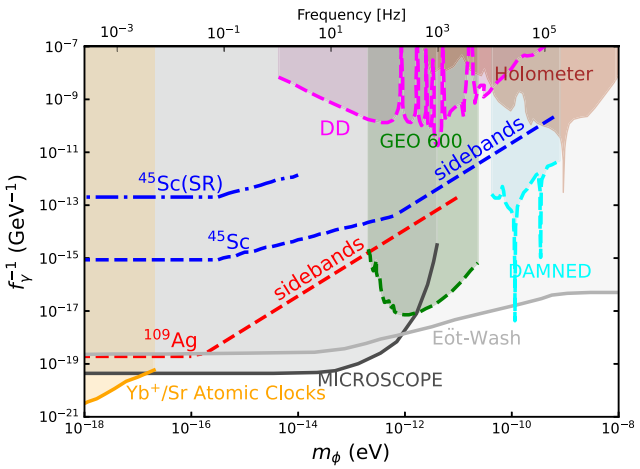


Fig. 3. (color online) Projected sensitivity to the scalar DM–photon coupling f_γ^{-1} as a function of the dark matter mass m_ϕ. The red and blue dashed lines denote the results for ^{109}Ag and ^{45}Sc, respectively. The blue dot-dashed line corresponds to ^{45}Sc(SR) with synchrotron radiation. Existing constraints from GEO 600 [42], DD [43], DAMNED [44], Holometer [45], Yb$^+$ and Sr atomic clocks [46–48], and equivalence-principle tests by MICROSCOPE [49, 50] and Eöt-Wash [51, 52] are shown for comparison. Approximate sideband sensitivities are also shown. For ^{109}Ag and ^{45}Sc using conventional radioactive sources, the source activity is fixed at 0.1 Ci. For ^{45}Sc with synchrotron radiation (SR), a spectral photon flux of $5\times10^{14}\,\mathrm{ph\,s^{-1}\,eV^{-1}}$ is assumed.

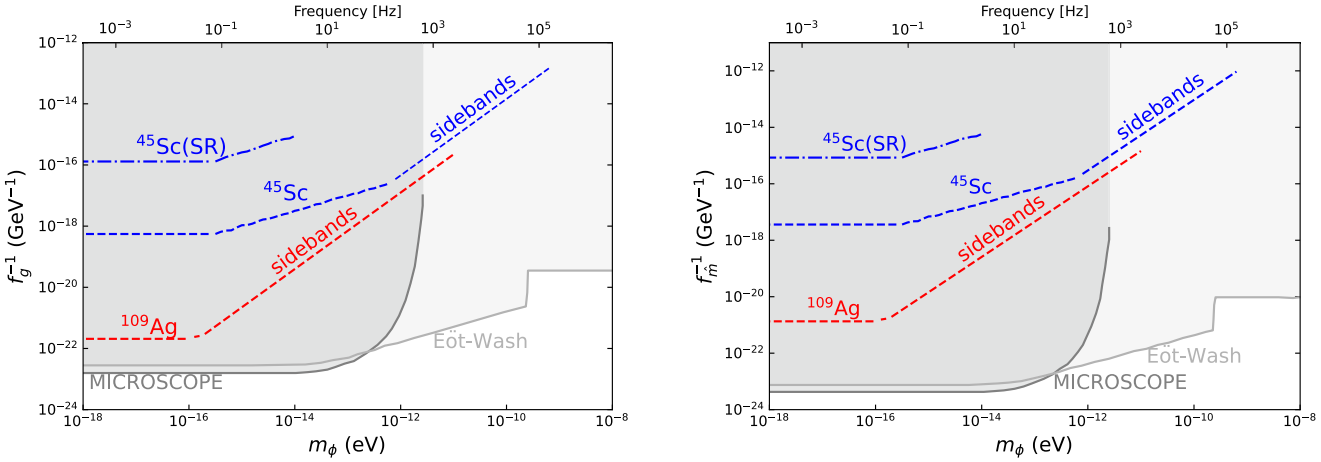


Fig. 4. (color online) Projected sensitivity to the scalar DM–gluon coupling f_g^{-1} (a) and the scalar DM–quark coupling $f_{\hat{m}}^{-1}$ (b) as functions of the dark matter mass m_ϕ. The red and blue dashed lines denote the results for ^{109}Ag and ^{45}Sc, respectively, while the blue dot-dashed line corresponds to ^{45}Sc with synchrotron radiation. Approximate sideband sensitivities are shown for comparison. Existing constraints from equivalence-principle tests by MICROSCOPE [49, 50] and Eöt-Wash [51, 52] are also shown.

corresponding constraints on the DM–photon coupling constant f_γ, shown in Fig. 3; the DM–gluon coupling constant f_g, shown in Fig. 4(a); and the DM–quark coupling constant $f_{\hat{m}}^{-1}$, shown in Fig. 4(b), at the 95% confidence level. The sensitivities shown here are based only on statistical uncertainties and do not include detector or systematic effects. In our analysis, we adopt the parameters listed in Table 1 and Table 2. For the traditional Mössbauer sources based on ^{109}Ag and ^{45}Sc, the experimentally measured linewidths are used in the transmission function given in Eq. (6). For the Mössbauer resonance of ^{45}Sc excited by synchrotron radiation, the nuclear resonance photon flux $N_\gamma^{\rm MS}$ in Eq. (14) is calculated using the natural linewidth, while the experimentally measured linewidth is adopted in the transmission function in Eq. (6).

Figure 3 shows the constraints on the scalar DM–photon coupling f_γ^{-1}. The red and blue dashed lines correspond to ^{109}Ag and ^{45}Sc using radioactive sources, respectively, while the blue dot-dashed line represents the constraint from ^{45}Sc using synchrotron radiation. For constraints obtained with Mössbauer radioactive sources, the dark matter mass cannot be arbitrarily small because the effective experimental integration time is limited by the lifetime of the parent isotope. This introduces a low-mass cutoff in the parameter space. Specifically, the dark matter oscillation period $2\pi/m_\phi$ must not exceed the lifetime of the parent nucleus t_P. For the ^{109}Ag system, the parent isotope is ^{109}Cd with lifetime $t_{\rm Cd}$, giving

$$m_\phi > 2\pi/t_{\rm Cd} \simeq 1.04\times10^{-22}{\rm eV}. \tag{24}$$

Similarly, for the ^{45}Sc system, the corresponding lower bound is $m_\phi > 2.94\times10^{-22}$ eV. At high dark matter masses, the sensitivity is limited by the requirement to obtain sufficient photon counts in each height bin at the 3σ level. In the SR scenario, the sensitivity is not constrained by the decay lifetime of a parent isotope, but rather by the realistic operation time available at the synchrotron facility. The ULDM field remains phase coherent for only one coherence time,

$$\tau \simeq 10^6\times\frac{2\pi}{m_\phi}. \tag{25}$$

For $m_\phi < 10^6\times2\pi/t_{\rm P}$ and $m_\phi \geq 10^6\times2\pi/t_{\rm P}$, we assume effective experimental integration times of $t_{\rm obs} = t_{\rm P}$ and $t_{\rm obs} = \tau$, respectively. In this work, we conservatively take the observation time to be one dark matter coherence time at high dark matter masses. Longer observation times, $t_{\rm obs} \gg \tau$, can provide multiple statistically independent measurements and further improve the sensitivity.

In Fig. 3, the red and blue dashed lines denote the projected sensitivities obtained with ^{109}Ag and ^{45}Sc radioactive sources, respectively, while the blue dot-dashed line corresponds to the result for ^{45}Sc using synchrotron radiation. For ^{109}Ag, the projected sensitivity can reach approximately 10^{-19} GeV^{-1}. For ^{45}Sc, the projected sensitivity is approximately 10^{-15} GeV^{-1} with a conventional radioactive source and about 10^{-13} GeV^{-1} in the SR-based configuration. The green shaded region indicates the GEO 600 bound [42], obtained through spectral analysis of strain data from the GEO 600 gravitational-wave interferometer. The magenta region shows the exclusion limit from Dynamical Decoupling (DD) [43], derived from the non-observation of variations in the fine-structure constant α caused by oscillating scalar dark matter in an

atomic optical transition. The cyan region represents the 'DArk Matter from Non Equal Delays' experiment bound [44], obtained from dark matter searches using an optical cavity with unequal-delay interferometry. The brown region shows the Holometer bound [45], derived by studying variations of the fine-structure constant α using cross-correlated data from the Fermilab Holometer instrument. The orange region represents constraints derived from Yb^+ and Sr atomic clock experiments [46–48]. The solid gray and light gray regions correspond to fifth-force (FF) and equivalence-principle (EP) tests, including the MICROSCOPE experiment [49–50] and the Cu/Pb torsion-pendulum experiment performed by the Eöt-Wash group [51–52], following Refs. [16, 53]. Among the nuclei considered here, ^{109}Ag provides the strongest sensitivity. In the high-mass region, its projected sensitivity surpasses the constraints from Dynamical Decoupling (DD), while in the low-mass region it approaches the current limits from EP tests, although it remains weaker than the bounds derived from Yb^+ and Sr atomic clock experiments.

As noted in Ref. [23], the homogeneous-shift approximation is valid when the dark matter oscillation period is longer than the nuclear lifetime, corresponding to the regime $m_\phi \lesssim \Gamma$. In this limit, the DM-induced energy shift can be treated as quasi-static and approximately uniform across the resonance line. For both ^{109}Ag and ^{45}Sc, the sensitivities presented in this work are valid in this regime. For $m_\phi \gtrsim \Gamma$, however, the rapid oscillation of the dark matter field leads to sidebands at $E_0 \pm n m_\phi$ ($n = \pm1, \pm2, \ldots$), rather than a simple homogeneous shift of the central resonance line. The modulation may manifest as effective symmetric broadening or as a small residual shift of the central resonance line. Consequently, the sensitivities would be reduced. As discussed in Ref. [54], the first sidebands located at $E_0 \pm m_\phi$ have intensities suppressed by a factor $\sim (\Delta E/2m_\phi)^2$, and the intensities of higher-order sidebands are further suppressed. If the sidebands become detectable, the shift energy ΔE could be constrained with a scaling $\propto m_\phi/N_{total}^{1/4}$. The corresponding sideband sensitivities in Figs. 3 and 4 should be regarded as order-of-magnitude estimates. In a dedicated analysis, one would combine the full dataset to reconstruct the complete absorption spectrum and search for the sideband structure around the central resonance frequency. Moreover, at higher dark matter masses, longer observation times, $t_{\rm obs} \gg \tau$, would provide multiple statistically independent measurements and further improve the sensitivity.

Similarly, the projected sensitivity can be estimated for scalar DM couplings to gluons and quarks. In each case, only one type of coupling is assumed to be present, while possible interference effects between different couplings are neglected. Figure 4(a) shows the projected constraints on the scalar DM–gluon coupling f_g^{-1}. The strongest reach is obtained with ^{109}Ag, for which the best projected sensitivity reaches approximately $10^{-22}\,\mathrm{GeV}^{-1}$. The constraints from ^{45}Sc are less stringent. Figure 4(b) presents the projected constraints on the scalar DM–quark coupling $f_{\hat{m}}^{-1}$. Similarly, ^{109}Ag yields the strongest sensitivity, with the best projected sensitivity reaching approximately $10^{-21}\,\mathrm{GeV}^{-1}$, while the constraints from ^{45}Sc remain weaker.

Among the nuclei considered, ^{109}Ag and ^{45}Sc, ^{109}Ag yields the strongest constraints on dark matter couplings, making it the most promising candidate for future precision experiments probing interactions between dark matter and the Standard Model. By contrast, ^{45}Sc with a conventional radioactive source provides comparatively weaker limits. Although the current constraints derived from ^{45}Sc using a synchrotron-radiation-based source are weaker than those obtained from ^{109}Ag, this approach offers several important advantages. In particular, the experimental integration time can be extended, and the photon flux may be substantially improved through future advances in synchrotron technology. An X-ray free-electron laser oscillator is a promising next-generation hard X-ray source capable of delivering fully coherent pulses with meV-level bandwidth and a highly stable flux expected to reach $1\times10^{15}\,\mathrm{ph\,s^{-1}\,meV^{-1}}$ [55]. If applied to dark matter searches, such improvements would substantially increase the number of available photons and could further enhance experimental sensitivity. Overall, ^{109}Ag provides the most stringent and robust constraints among the nuclei considered, highlighting its strong potential for future high-precision probes of dark matter interactions with the Standard Model.

VII. CONCLUSIONS AND DISCUSSION

The Mössbauer effect is a powerful tool for detecting small shifts in nuclear energy levels. In this study, we explore its potential for probing the coupling between dark matter and nuclei in the source and absorber of a Mössbauer spectrometer. To investigate possible variations in nuclear transition energies induced by an oscillating dark matter background, we consider a static Mössbauer measurement scheme. Ultralight dark matter interacting with both the emitter and absorber can induce variations in their nuclear energy levels, resulting in a measurable shift in the position of the Mössbauer resonance.

In our analysis, we select ^{109}Ag and ^{45}Sc as candidate Mössbauer isotopes. We assume an emitter source with an activity of $A = 0.1\,\mathrm{Ci}\,(3.7\,\mathrm{GBq})$ and also consider ^{45}Sc in a synchrotron-radiation scheme. The baseline distance between the emitter and absorber for ^{109}Ag and ^{45}Sc is $L = 1\,m$. The DM mass is varied over the range from 10^{-20}eV to 10^{-8} eV. Under these assumptions, we derive projected constraints on the DM–photon coupling f_γ^{-1},

the DM–gluon coupling f_g^{-1}, and the DM–quark coupling $f_{\hat{m}}^{-1}$.

Among the isotopes considered in this work, ^{109}Ag provides the strongest sensitivity, whereas ^{45}Sc yields comparatively weaker constraints, with the synchrotron-radiation-based ^{45}Sc setup giving the weakest reach. For ^{109}Ag, the projected sensitivity to the scalar DM–photon coupling f_γ^{-1} reaches approximately $10^{-19}\,\mathrm{GeV}^{-1}$, approaching the current limits from EP tests. For the scalar DM–gluon coupling f_g^{-1} and the scalar DM–quark coupling $f_{\hat{m}}^{-1}$, the projected sensitivities of ^{109}Ag reach approximately 10^{-22} and $10^{-21}\,\mathrm{GeV}^{-1}$, respectively. Although the physically viable parameter space accessible in the present study is already covered by existing experimental constraints from equivalence principle tests, searches based on the Mössbauer effect provide a complementary experimental avenue for probing ultralight dark matter. Owing to their distinct detection principle and ultrahigh energy resolution, such experiments offer an independent test of scalar dark matter interactions and broaden the range of experimental techniques available for exploring physics beyond the Standard Model.

The ^{67}Zn isotope can also be considered as an alternative candidate. Its 93.3 keV transition has a relatively narrow experimental linewidth of 7.5×10^{-11} eV [21], which leads to a gravitational broadening of $\delta Z = 7.4$ m. Accordingly, the detector spatial resolution would need to be set to 3.7 m. This would require a longer baseline and a larger detector, and photon number attenuation over the long propagation distance must also be taken into account. Although this transition could in principle provide meaningful constraints, its experimental feasibility remains challenging. Future studies could explore the potential of ^{67}Zn for such measurements.

Further enhancements could be achieved by increasing the source activity and incorporating optic control, both of which would increase the number of detected photons and thereby improve photon statistics. In light of future powerful synchrotron radiation sources delivering high-brightness X-ray beams, synchrotron-based Mössbauer spectroscopy has become increasingly important. In particular, the development of narrow-band, high-repetition-rate XFELs has enabled resonant excitation of ^{45}Sc, as recently demonstrated at the European XFEL. If such technology were applied to dark matter searches, it could substantially increase the number of emitted photons and further enhance the experimental sensitivity.

ACKNOWLEDGMENTS

The authors thank Hua-Qiao Zhang, Xing-Jian Lv, and Han Miao for valuable discussions. During the preparation of this paper, [56] appeared, focusing on the pseudoscalar type of ultralight dark matter.

References

[1] N. Aghanim *et al.* (Planck Collaboration), Astron. Astrophys. **641**, A6 (2020) [Erratum: Astron. Astrophys. **652**, C4 (2021)], arXiv: 1807.06209[astro-ph.CO]
[2] E. Corbelli and P. Salucci, Mon. Not. Roy. Astron. Soc. **311**, 441 (2000), arXiv: astro-ph/9909252
[3] D. Clowe, M. Bradac, A. H. Gonzalez *et al.*, Astrophys. J. Lett. **648**, L109 (2006), arXiv: astro-ph/0608407
[4] D. Clowe, A. Gonzalez, and M. Markevitch, Astrophys. J. **604**, 596 (2004), arXiv: astro-ph/0312273
[5] M. Markevitch, A. H. Gonzalez, L. David *et al.*, Astrophys. J. Lett. **567**, L27 (2002), arXiv: astro-ph/0110468
[6] G. Jungman, M. Kamionkowski, and K. Griest, Phys. Rept. **267**, 195 (1996), arXiv: hep-ph/9506380
[7] E. G. M. Ferreira, Astron. Astrophys. Rev. **29**, 7 (2021), arXiv: 2005.03254[astro-ph.CO]
[8] M. S. Safronova, D. Budker, D. DeMille *et al.*, Rev. Mod. Phys. **90**, 025008 (2018), arXiv: 1710.01833[physics.atom-ph]
[9] D. Antypas, D. Budker, V. V. Flambaum *et al.*, Annalen Phys. **532**, 1900566 (2020), arXiv: 1912.01335 [physics.atom-ph]
[10] T. Damour and A. M. Polyakov, Nucl. Phys. B **423**, 532 (1994), arXiv: hep-th/9401069
[11] J. D. Barrow, Phys. Rev. D **59**, 043515 (1999)
[12] H. B. Sandvik, J. D. Barrow, and J. Magueijo, Phys. Rev. Lett. **88**, 031302 (2002), arXiv: astro-ph/0107512
[13] A. Arvanitaki, J. Huang, and K. Van Tilburg, Phys. Rev. D **91**, 015015 (2015), arXiv: 1405.2925[hep-ph]
[14] Y. V. Stadnik and V. V. Flambaum, Phys. Rev. Lett. **115**, 201301 (2015), arXiv: 1503.08540[astro-ph.CO]
[15] A. Banerjee, H. Kim, and G. Perez, Phys. Rev. D **100**, 115026 (2019), arXiv: 1810.01889[hep-ph]
[16] A. Hees, O. Minazzoli, E. Savalle *et al.*, Phys. Rev. D **98**, 064051 (2018), arXiv: 1807.04512[gr-qc]
[17] E. Savalle, B. M. Roberts, F. Frank *et al.*, (2019), arXiv: 1902.07192[gr-qc]
[18] R. L. Mössbauer, Z. Phys. **151**, 124 (1958)
[19] T. Katila and K. Riski, Phys. Lett. A **83**, 51 (1981)
[20] W. Potzel, C. Schäfer, M. Steiner *et al.*, Hyperfine Interact **72**, 195 (1992)
[21] G. Gratta, D. E. Kaplan, and S. Rajendran, Phys. Rev. D **102**, 115031 (2020), arXiv: 2010.03588[hep-ph]
[22] Y. Gao, H. Zhang, and W. Xu, Sci. Bull. **69**, 2795 (2024), arXiv: 2310.06607[gr-qc]
[23] A. Banerjee, (2024), arXiv: 2408.04700[hep-ph]
[24] M. E. D. Center, *Properties of isotopes relevant to mossbauer spectroscopy*, http://www.medc.dicp.ac.cn/Resources.htm (2025), accessed: 07, 11, (2025)
[25] D. Griesinger, R. V. Pound, and W. Vetterling, Phys. Rev. B **15**, 3291 (1977)
[26] Y. Shvyd'ko, R. Röhlsberger, O. Kocharovskaya *et al.*, Nature **622**, 471 (2023)
[27] W. Decking *et al.*, Nature Photon. **14**, 391 (2020)
[28] S. Liu, C. Grech, M. Guetg *et al.*, Nature Photonics **17**, 984 (2023)
[29] J. Wan, Y. Leng, B. Gao *et al.*, Nucl. Instrum. Meth. A

1026, 166200 (2022)
[30] Z. T. Zhao, C. Feng, and K. Q. Zhang, Nucl. Sci. Tech. **28**, 117 (2017)
[31] Z. Zhao, C. Feng, J. Chen *et al*., Sci. Bull. **61**, 720 (2016)
[32] X. Wang *et al*., JACoW **IPAC2023**, TUPL043 (2023)
[33] Z. Li, J. Shao, H. Qizhang *et al*., JACoW **LINAC2024**, TUPB048 (2024)
[34] P. Liu *et al*., *Probing the linewidth of the 12.4-kev solid-state ^{45}sc isomeric resonance*, (2025), arXiv: 2508.17538[quant-ph]
[35] P. Gütlich, E. Bill, and A. X. Trautwein, *Mössbauer Spectroscopy and Transition Metal Chemistry: Fundamentals and Applications*, (Springer, 2011)
[36] W. Sturhahn, J. Phys.: Condens. Mat. **16**, S497 (2004)
[37] K. Zhang *et al*., J. Synchrotron Radiat. **33**, 429 (2026)
[38] J. P. Sutter, S. G. Alcock, F. Rust *et al*., in *Adaptive X-Ray Optics III*, Vol. 9208, edited by S. L. O'Dell and A. M. Khounsary, International Society for Optics and Photonics (SPIE, 2014) p. 92080G
[39] G. J. Long, T. E. Cranshaw, and G. Longworth, Mössbauer Effect Reference and Data Journal **6**, 42 (1983)
[40] W. Wildner and U. Gonser, Le Journal De Physique Colloques, 40, (1979)
[41] https://www-nds.iaea.org/relnsd/vcharthtml/VChartHTML.html.
[42] S. M. Vermeulen *et al*., Nature **600**, 424 (2021)
[43] S. Aharony, N. Akerman, R. Ozeri *et al*., Phys. Rev. D **103**, 075017 (2021), arXiv: 1902.02788[hep-ph]
[44] E. Savalle, A. Hees, F. Frank *et al*., Phys. Rev. Lett. **126**, 051301 (2021), arXiv: 2006.07055[gr-qc]
[45] L. Aiello, J. W. Richardson, S. M. Vermeulen *et al*., Phys. Rev. Lett. **128**, 121101 (2022), arXiv: 2108.04746[gr-qc]
[46] N. Sherrill *et al*., New J. Phys. **25**, 093012 (2023), arXiv: 2302.04565[physics.atom-ph]
[47] M. Filzinger, S. Dörscher, R. Lange *et al*., Phys. Rev. Lett. **130**, 253001 (2023), arXiv: 2301.03433[physics.atom-ph]
[48] J. Arakawa *et al*., (2026), arXiv: 2602.16804[hep-ph]
[49] P. Touboul *et al*., Phys. Rev. Lett. **119**, 231101 (2017), arXiv: 1712.01176[astro-ph.IM]
[50] J. Bergé, P. Brax, G. Métris *et al*., Phys. Rev. Lett. **120**, 141101 (2018), arXiv: 1712.00483[gr-qc]
[51] G. L. Smith, C. D. Hoyle, J. H. Gundlach *et al*., Phys. Rev. D **61**, 022001 (2000), arXiv: 2405.10982[gr-qc]
[52] S. Schlamminger, K. Y. Choi, T. A. Wagner *et al*., Phys. Rev. Lett. **100**, 041101 (2008), arXiv: 0712.0607[gr-qc]
[53] H. Banks, E. Fuchs, and M. McCullough, (2024), arXiv: 2407.11112[hep-ph]
[54] E. Fuchs, F. Kirk, E. Madge *et al*., Phys. Rev. X **15**, 021055 (2025), arXiv: 2407.15924[hep-ph]
[55] B. Adams *et al*., (2019), arXiv: 1903.09317 [physics.insdet]
[56] S. Liu, K. F. Lyu, J. Meng *et al*., (2025), arXiv: 2511.14851[hep-ph]